Capacitance-Based Sensor with Layered Carbon-Fiber Reinforced Polymer and Titania-Filled Epoxy

Jin Yan[a], Austin Downey[b], An Chen[a,*], Simon Laflamme[a,c], Sammy Hassan[a]

[a]*Department of Civil, Construction, and Environmental Engineering, Iowa State University, Ames, IA, USA;*
[b]*Department of Mechanical Engineering, University of South Carolina, Columbia, SC, USA;*
[c]*Department of Electrical and Computer Engineering, Iowa State University, Ames, IA, USA*

Abstract

Advances in intelligent infrastructure can be achieved through the use of novel materials for increased system-level efficiency and multifunctionality. Carbon Fiber-Reinforced Polymer (CFRP) has been widely used in strengthening, rehabilitating, and retrofitting of existing structures because of its speed of deployment, low maintenance requirement, and high strength-to-weight ratio. In this work, the authors propose a novel method to augment CFRP with self-sensing capabilities. The sensor consists of two CFRP layers separated by a titania-filled epoxy dielectric layer, therefore forming a parallel plate capacitor. Sensing capability can be achieved through variations in the sensor's capacitance provoked by strain, therefore providing an additional function that could be leveraged for structural health monitoring and structural health management purposes. Comprehensive testing, including (1) sensing properties on sensors with and without titania-doped epoxy and (2) electromechanical test on tension specimens subjected to both static and dynamic loading, was conducted. The test results show that doping the titania filler within the epoxy matrix can improve the sensor's sensitivity and that the sensor's signal increases linearly with increasing strain. A static gauge factor of 0.92 was obtained, and the dynamic gauge factor characterized under 0.25, 0.5, and 1Hz. It is also found that CFRP can be used as a self-sensing material without affecting its mechanical properties.

Keywords: Capacitor; Multifunctional material; Strain sensing; Carbon fiber reinforced polymer; Composite; Structural health monitoring.

1. Introduction

Structural health management of civil infrastructure is typically conducted through maintenance operations that are scheduled based on condition reports resulting from visual inspections. These visual inspections are sometimes accompanied by non-destructive evaluation (NDE) techniques to enhance the damage detection and quantification capabilities. However, both visual inspection and NDE processes are expensive and time-consuming. Structural health monitoring (SHM) is the automation of these processes, where a sensing system combined with signal processing and decision making algorithms can be leveraged to enable the online discovery of changes in structural health [1] and condition-based maintenance decisions [2]. A range of different technologies using wireless sensor networks [3, 4] and dense sensor arrays [5, 6] have been investigated for SHM applications. However, these methods are generally expensive to deploy and full-scale cost-effectiveness have yet to be demonstrated. Effective integration of structural components and sensors in the form of multifunctional materials has the potential to create cost-effective SHM solutions.

*Corresponding author
Email addresses: yanjin@iastate.edu (Jin Yan), ADOWNEY2@cec.sc.edu (Austin Downey), achen@iastate.edu (An Chen), laflamme@iastate.edu (Simon Laflamme)

Multifunctional materials have recently gained popularity in the research community [7]. An approach to the development of such materials is the integration of sensor networks within the material matrix to create a smart material. A considerable number of investigations have been conducted on fiber optic [8] sensors, piezoelectric sensors [9], sensory textiles [10] and inkjet printed films [11] to detect damage. Other solutions focus on the integration of nanofillers and nanoadditives to rethink traditional concretes [12, 13] and bricks [14, 15] into multifunctional components.

Of interest to this paper are multifunctional materials based on carbon fiber reinforced polymers (CFRPs). CFRP materials have been widely used for the strengthening, rehabilitating and retrofitting of structures due to their high strength-to-weight ratio, long service life, and high abrasion and wear resistance [16, 17]. Early research on augmenting CFRPs with additional functions leveraged the carbon fibers' piezoresistive effect for self-sensing capabilities [18, 19, 20]. Self-sensing is provided by changes in electrical resistance of the CFRP associated with its deformation, ideal for strain measurements. Several studies have attempted to improve the electrical resistance-based self-sensing behavior [21] by enhancing the electrical contact at the electrodes [22], and the measurement methods [23]. Others have proposed CFRP-based structural supercapacitors for energy harvesting capabilities. Chung and Wang [24] proposed a capacitor fabricated from semi-conductive carbon fibers for the electrodes and an insulation paper for the dielectric. Luo and Chung [25] proposed using pre-preg CFRP layers for the electrodes and insulation paper for the dielectric, demonstrating a capacitance up to 1200 nF/m^2. Other research studied the use of different separators for creating dielectrics [26] and different treatment of surface electrodes [27].

CFRP-based capacitors have recently attracted interest for self-sensing capabilities, where changes in the material's geometry provoke a change in the electrical capacitance. Unlike electrical resistance-based CFRP, the literature on capacitance-based CFRP is limited. Carlson and Asp [28] studied the effect of damage on the electrical properties of a structural capacitor that used polyethylene terephthalate (PET) for the dielectric. They reported that the capacitance remained unchanged after significant interlaminar matrix cracking in the CFRP electrodes. Shen and Zhou [29] discussed that interlaminar damage can instead lead to a reduction in capacitance, and modeled the capacitance as a function of interfacial cracking. It was also noted in [30] that low capacitance values may complicate field applications, because of the challenge associated with the measurement of small changes in electrical capacitance, whereas CFRP supercapacitors could be more suited for SHM applications.

In this work, the authors propose a novel CFRP-based capacitor to provide the CFRP's self-sensing functionality. The objective is to develop a CFRP sensor that exhibits a linear increase in capacitance over strain, consistent with previous results obtained by the authors on self-sensing capacitors [31]. The sensor leverages CFRP to form the electrodes of the capacitor, while the dielectric is formed by a titania-filled epoxy layer. Epoxy resin has been commonly used for electrical insulation and is a suitable matrix for the improvement of electrical energy storage through the addition of nanoparticles [32]. The dispersion of titania results in a significant increase of permittivity and preserves the low dielectric loss of the epoxy resin [33]. By adding the sensing function, different from other pure sensing strategies, CFRP becomes a multifunctional material without affecting its original mechanical properties, which can be used for both load bearing and self-sensing. This technology is especially useful for CFRP applications, since CFRP typically covers a large continuous area of which SHM technologies are difficult to apply due to technical and economic challenges.

The rest of the paper is organized as follows. First, the sensor materials and its fabrication process are presented, along with its electromechanical model. Second, the experimental procedures are introduced, and experimental results on the mechanical and electromechanical behaviors are presented and discussed. Lastly, the paper is concluded.

2. Background

2.1. Sensor materials

Fabric MBrace® CF130 and epoxy MBrace® Saturant were acquired from BASF Construction Chemicals. A unidirectional alignment carbon fiber pattern of an ultimate tensile strength of 3,800 MPa was selected. The mechanical properties of the CFRP components are listed in Table 1. Polydimethylsiloxane (PDMS) coated titania was acquired from TPL inc.

Table 1: Mechanical properties of CFRP components provided by the supplier

Component	Young's [1] Modulus (GPa)	Fiber-based [1] Ultimate Strength (MPa)	Laminate-based [2] Ultimate Strength (MPa)	Rupture Strain (%)
Saturant	3.034	55.2	-	3.50%
Cured CF130 laminate	227	3800	627 - 1045	1.67%

[1] These values are obtained by testing cured laminates (per ASTM D3039) and dividing the resulting strength and modulus per unit width by the nominal fiber thickness (0.165 mm for one layer of CF130 fiber).

[2] These values are obtained by testing cured laminates (per ASTM D3039) and dividing the resulting strength and modulus per unit width by the total cured thickness (0.6 to 1.0 mm for laminate containing one layer of CF130 fiber).

2.2. Sensor fabrication

The CFRP capacitor is composed of two conductive electrodes separated by a dielectric, fabricated using the following two-step process:

1. *CFRP electrode fabrication* (Figure 1(a)): The bi-component epoxy is made by mixing part A to part B at a weight ratio 3:1 using a low-speed homogenizer (600 rpm) for 3 minutes. The uncured epoxy is applied to the fabric and cured using a vacuum bagging process. Two copper tapes with conductive adhesive are attached on the top and bottom of the fabric surface before applying the epoxy to provide electrical contact to the DAQ. The surface of the copper tape is polished with sandpaper after curing to remove any excess epoxy. The electrode plates are cured for 24 hours.
2. *Sensor assembly* (Figure 1(b)): The capacitor is assembled by separating two cured CFRP plates by a dielectric layer. The dielectric is fabricated using the same epoxy but filled with titania to increase the dielectric permittivity. Titania rutile particles are dispersed in the epoxy at 5% by weight and mixed using a low-speed homogenizer (600 rpm) for 5 minutes to obtain a uniform dispersion. The titania-doped epoxy is applied to one cured plate and another cured plate is then placed on top of the epoxy layer to sandwich the epoxy layer between the two cured plates. Thereafter, the specimen is cured for 24 hours using a vacuum bagging process.

After assembly, the specimen was cut into 25.4 mm (1 in) wide strips using a table saw. The edges were trimmed to avoid uneven thicknesses and provide consistent electrical conductance and capacitance. The specimens were further sanded to prevent electrodes from forming an electrical short at the edges. The CFRP sensor layers are schematized in Figure 2(a).

2.3. Sensing principle

The capacitance (C) of a CFRP parallel plate capacitor can be modeled as a non-lossy parallel plate capacitor assuming an electrical excitation test frequency of less than 1 kHz:

$$C = e_0 e_r \frac{A}{h} \tag{1}$$

where $e_0 = 8.854$ pF/m is the vacuum permittivity, e_r is the polymer's relative permittivity, $A = w \cdot l$ is the sensor area of width w and length l, and h is the thickness of the dielectric as annotated in Figure 2(b).

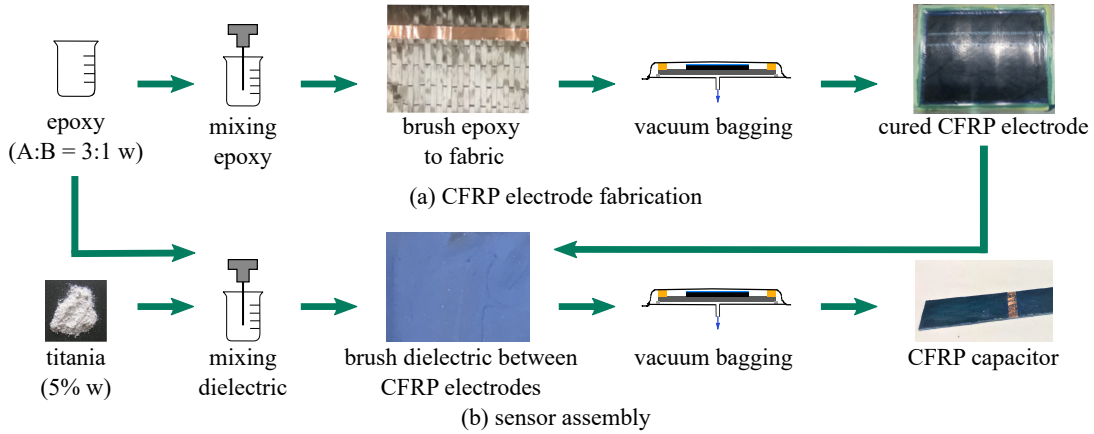

Figure 1: CFRP sensor fabrication process: (a) fabrication of the CFRP electrodes; and (b) assembly of the sensor.

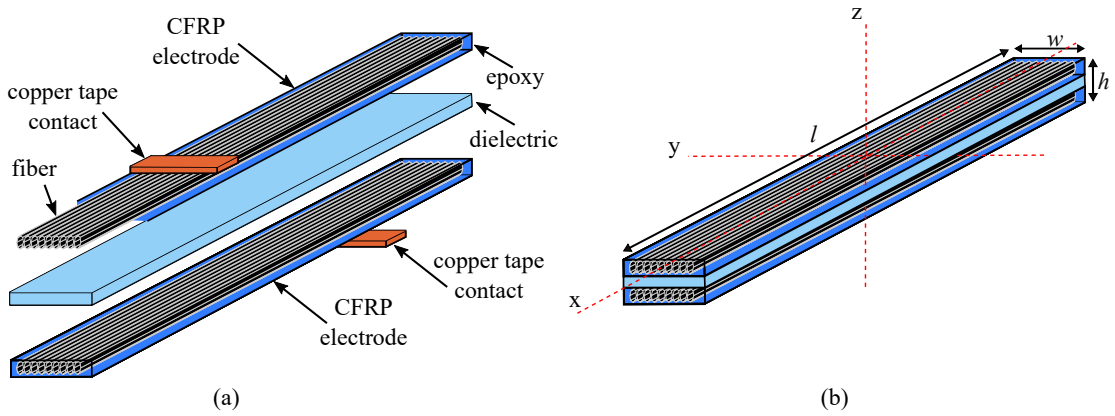

Figure 2: (a) Schematic of CFRP sensor layers; and (b) annotations for sensing principle.

Adapting the model of an ideal dielectric elastomer [34] and assuming the electric displacement is taken to be linear in the electric field and independent of the state of deformation, the capacitance change is linear and relates only to the strain applied to the capacitor. When the capacitor is subjected to a small change in strain, differentiation of Equation (1) leads to an expression that relates a change in strain to a change in capacitance (ΔC) [6]:

$$\begin{aligned} \frac{\Delta C}{C} &= \frac{\Delta l}{l} + \frac{\Delta w}{w} - \frac{\Delta h}{h} \\ &= \varepsilon_{\mathrm{x}} + \varepsilon_{\mathrm{y}} - \varepsilon_{\mathrm{z}} \end{aligned} \tag{2}$$

where $\Delta l/l$, $\Delta w/w$, and $\Delta h/h$, can be expressed as strain ε_{x}, ε_{y}, and ε_{z}, respectively. In the coordinate system shown in Figure 2(b), axes x and y indicate the along fiber and transverse directions, respectively, and z the along the thickness direction. The increase in capacitance subject to a uniaxial planar strain occurs because of the increase of the interface area between CFRP electrodes and decrease of their relative distance.

The CFRP fibers in this study are unidirectional and as such the fabric is treated as orthotropic, where the properties along the fiber differ significantly from those across the fiber. Using Hooke's law under plane stress assumption, the out-of-plane strain ε_{z} and transverse strain ε_{y} can be written as a function of

longitudinal strain ε_x:

$$\begin{aligned} \varepsilon_y &= -\nu_{xy}\varepsilon_x \\ \varepsilon_z &= -\nu_{xz}\varepsilon_x \end{aligned} \tag{3}$$

The Poisson's ratio along the x-y plane ν_{xy} is assumed to be governed by the fiber while the out-of-plane Poisson's ratio ν_{xz} is assumed to be governed by the epoxy. Using these assumptions and combining Equations (2) and (3), the relative change in capacitance ΔC for the sensor subjected to longitudinal strain along the fiber can be related to a change in the sensor's deformation as:

$$\frac{\Delta C}{C} = (1 - \nu_{xy} + \nu_{xz})\varepsilon_x \tag{4}$$

which yields an expression for the gauge factor λ:

$$\lambda = \frac{\Delta C/C}{\varepsilon_x} = 1 - \nu_{xy} + \nu_{xz} \tag{5}$$

The theoretical gauge factor for uniaxial tensile strain applied to a parallel plate capacitor is a combination of the through-thickness and transverse Poisson's ratios. Equation (5) assumes that capacitance solely varies as a function of strain, the effect of permittivity is negligible, and there is no loss of strain between the electrodes and the dielectric layer. However, the gauge factor can also be influenced by the mounting method of the sensor, shear lag loss in the finite thickness, and operating conditions [35]. In this paper, the gauge factors of the specimens are obtained experimentally. It follows that the application of such a sensor would require a more constant fabrication process and/or calibration in the field.

3. Experimental Investigations

A series of tensile tests were conducted on five specimens (CF130 #1-#5) in order to characterize the electromechanical properties of the CFRP capacitor. Tests comprised quasi-static displacement-controlled tensile load and cyclic loads under various frequencies. All specimens were subjected to the same loading protocol. The following subsections introduce the experimental setup and present and discuss the experimental results.

3.1. Experimental setup

The experimental setup is shown in Figure 3, similar to the FRP strength evaluation experiments in [36, 37]. The specimens were 203 mm (8 in) long by 25.4 mm (1 in) wide, of variable thicknesses between specimens (reported in Table 3) due to the in-laboratory fabrication process. Fiberglass tabs were sanded and adhered onto the ends of the specimens to insulate the electrode from the hydraulic grip and provide protection against crushing. In the quasi-static tensile tests, a displacement-controlled load at a loading rate of 2 mm/min was applied using a servo-hydraulic testing machine (MTS model 312.41) with a TestStar IIm controller. Load and displacement data were acquired from the testing machine at a sampling frequency of 10 Hz until failure. CFRP capacitance measurements were performed using an LCR meter (Agilent 4263B). The LCR meter's built-in function to measure capacitance as a series of equivalent circuits were used in the test at a test frequency of 1 kHz. The specimens were equipped with a resistive strain gauge (RSG, model #FLA-30-11-1LJCT, manufactured by Tokyo Sokki Kenkyujo) at mid-height to obtain experimental values for the gauge factor. The RSG consisted of a foil gauge sampled at 10 Hz using a Vishay Model 5100 B Scanner DAQ. Data were filtered using a low-pass filter and zeroed using the average capacitance before loading. Lastly, a camera (Nikon D7100) was used to record high-resolution videos of the specimens during testing.

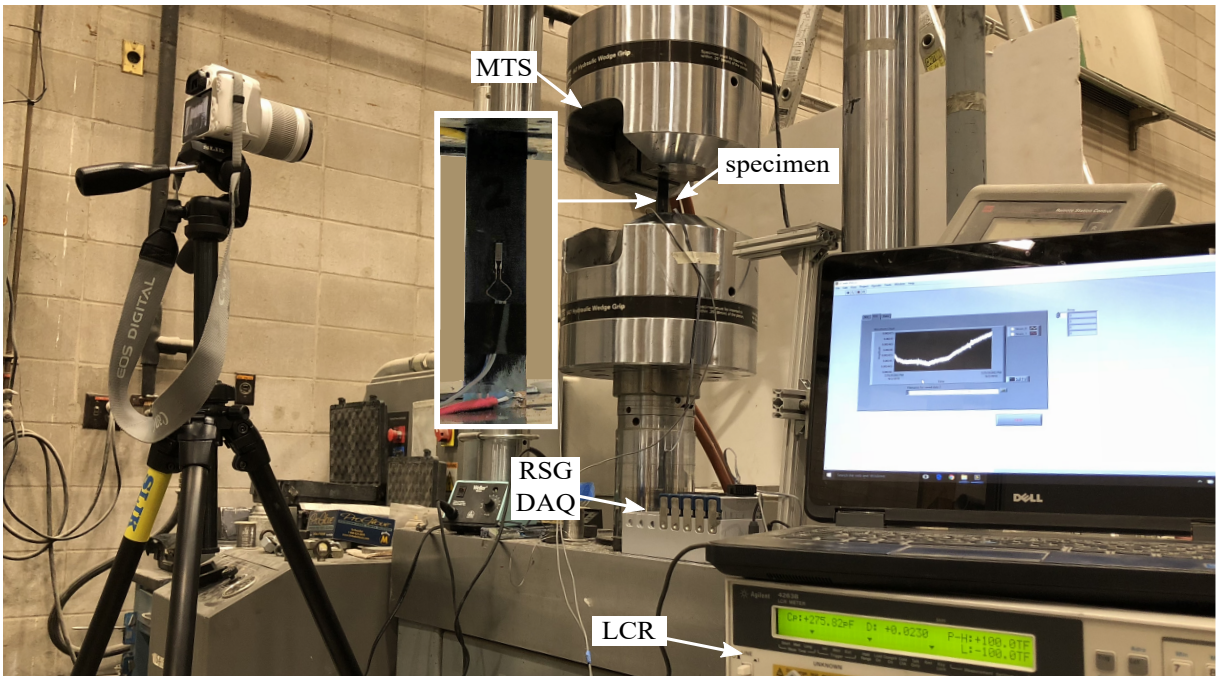

Figure 3: Experimental test setup for electromechanical characterization.

3.2. Titania-filled epoxy for enhanced sensing properties

The characteristics of CFRP capacitor with titanium-doped epoxy were compared with that of CFRP capacitor with the pristine dielectric to demonstrate the improvement of sensing properties. Samples measuring 25.4 × 25.4 mm^2 (1 × 1 in^2) were produced for the study. The relative permittivity (e_r) was measured using a test frequency of 1 kHz, and results listed in Table 2. The addition of titania at a concentration of 5% improved the relative permittivity of the specimen by 21%, and thus its sensitivity to strain. The long-term stability of the sensors was also studied. Figure 4(a) plots the relative change in capacitance for both sensors, and Figure 4(b) presents the same data in the form of fitted Gaussian probability density functions (PDFs). Results show that the addition of titania substantially decreased noise and significantly reduced the initial drift in the signal. This can be attributed to a smaller dielectric loss and a higher permittivity that results in better shielding against electromagnetic interference [32].

Table 2: Summary of sensor properties.

Dielectric	Capacitance (nF/mm^2)	Thickness (mm)	Relative permittivity e_r
Pristine	31.09	0.91	3.19
5% TiO2	36.78	0.93	3.86

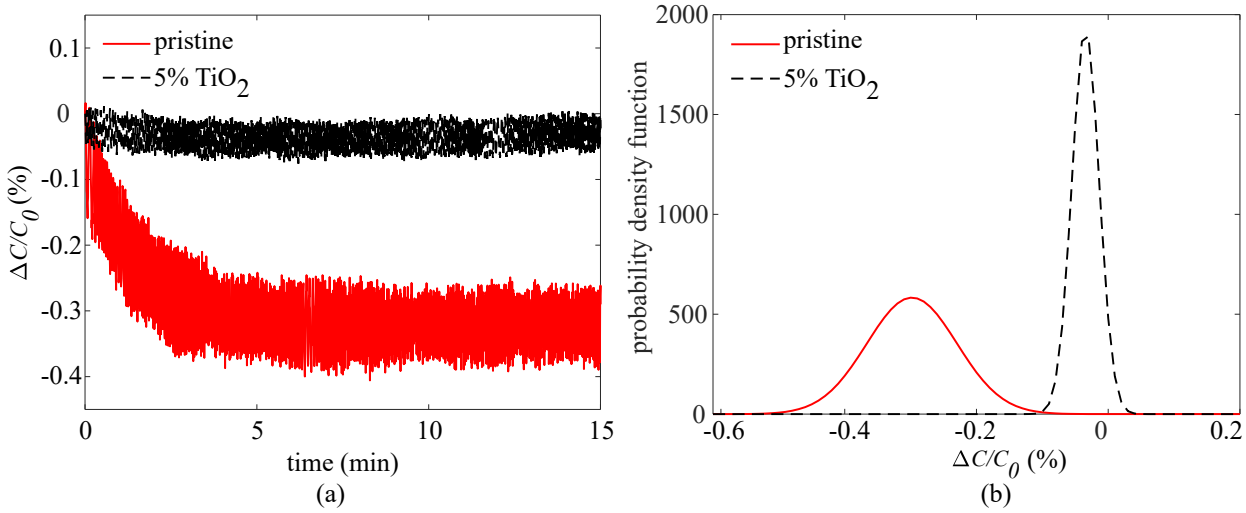

Figure 4: Long-term signal comparison: (a) time series signals; and (b) Gaussian probability density functions.

3.3. Electromechanical behavior

The stress-strain curves from the quasi-static tensile tests are plotted in Figure 5(a). The specimens were tested in tension until failure. It can be observed from Figure 5(a) that all specimens exhibit a linear stress-strain relationship before the brittle failure. The ultimate strength of the material was determined from the maximum load before the final failure/fracture. The calculated mechanical properties are listed in Table 3. The manufacturer provided the tensile modulus and strength based on the nominal fiber thickness for design purpose, as shown in 1. Following the same method, the average tensile modulus and strength for the specimens are calculated and shown in Table 3, which are increased by 15% and 12%, respectively, compared to results reported in Table 1. Therefore, the added titania-filled epoxy layer provoked an increase in the ultimate load. The strength and modulus with CF130 #2 are lower than the other specimens, which may be attributed to the higher thickness of the soft epoxy dielectric layer, and the residual stresses resulting from the mechanical processing and curing procedures [29]. Other than the method used by the manufacturer, another method is to calculate the ultimate strength based on the thickness of the cured laminate. Following this method, the strength of CFRP capacitors ranges from 504 - 791 MPa, which is below the range of the ultimate strength of pristine CFRP laminate, 627 - 1045 MPa, from Table 1, since CFRP capacitors are thicker than pristine CFRP laminates but contain the same amount of the fiber. Therefore, the strength and reinforcing effect of CFRP capacitors are affected by the amount of the dielectric layer.

To characterize the sensing capability of the CFRP capacitors, the capacitance time histories for each specimen were recorded. The baseline capacitance measurements C_0 (summarized in Table 3) were performed before the tests in an un-strained condition. Figure 5(b) plots the relative capacitance change ($\Delta C/C_0$) versus the applied strain measured by the RSGs. It can be observed that the relative change of capacitance increased with an increase in tensile strain. The CFRP capacitors lost its sensing function immediately after fracture. Also, all specimens showed comparable linear sensitivity to strain. The gauge factor for each specimen was obtained by conducting a linear fit through a least squares estimator. Results are listed in Table 3, and show a relatively similar gauge factor across samples, with an average $\lambda = 0.92$.

Post-damage inspection of the specimens was recorded by the camera. Figure 6(a) shows the typical failure modes of the specimens from the side and front view. The failure mechanisms were visually observed during testing and microcracks initializing in the composite matrix as the load increased were audible. Once the fibers started to break, the specimens would fail with a transverse fracture. In order to examine the microstructure damage of the carbon fiber fabrics, scanning electron microscopy (SEM) images of fractured specimens, operating at 15 kV without sputtering coating, were used for characterization. The polymer

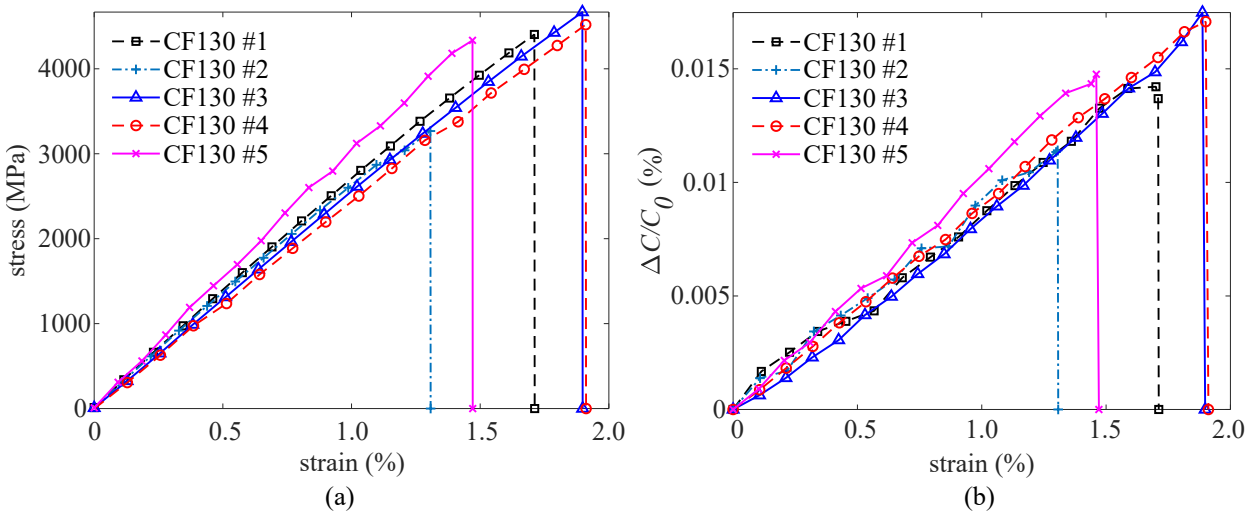

Figure 5: (a) stress versus strain curves; and (b) relative change in capacitance versus strain.

Table 3: Electrical-mechanical characterization of the specimens.

Specimen	Young's [1] Modulus (GPa)	Fiber-based [1] Ultimate Strength (MPa)	Laminate-based [2] Ultimate Strength (MPa)	Fracture Strain (%)	Total Thickness (mm)	Initial Capacitance (pF)	Gauge Factor
CF130 #1	258	4406	699	1.71	2.08	230	0.87
CF130 #2	253	3269	504	1.31	2.14	186	0.87
CF130 #3	248	4672	791	1.90	1.95	228	0.92
CF130 #4	239	4523	761	1.91	1.96	322	0.92
CF130 #5	297	4334	688	1.47	2.08	231	1.02
Average	259	4261	689	1.66	2.04	240	0.92

[1] Values are obtained by dividing the resulting strength and modulus per unit width by the nominal fiber thickness (0.33 mm for two layers of CF130 fiber).

[2] Values are obtained by dividing the resulting strength and modulus per unit width by the total (cured) thickness.

matrix between carbon fibers within the fiber bundles debonded as seen in Figure 6(b). Fiber breakage is shown in Figure 6(c).

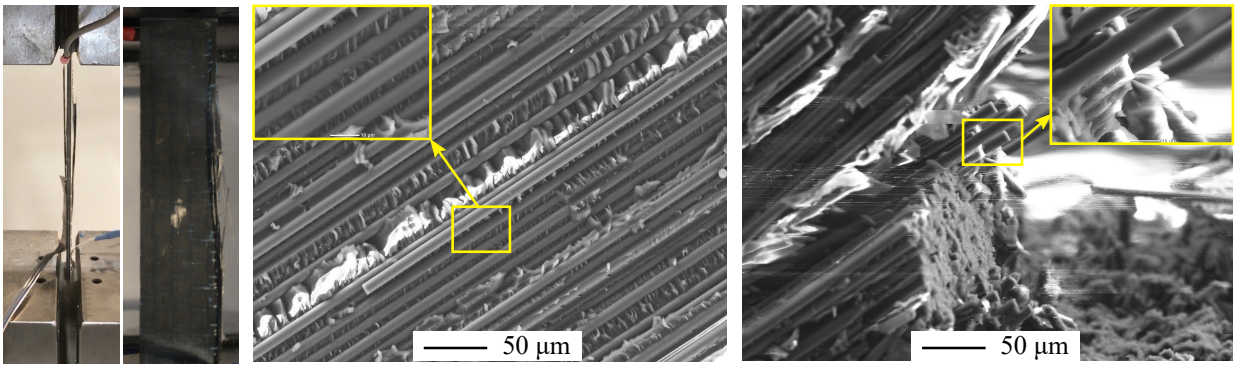

Figure 6: (a) Picture of a typical fiber fracture the from the side (left) and front (right) views; (b) SEM image of debonding between carbon fiber bundle and polymer matrix; and (c) SEM image of fiber breakage.

3.4. Cyclic load tests

To further investigate the stability and reversibility of the strain sensing under harmonic excitations, a series of cyclic tests were conducted on an additional specimen of 1.94 mm thickness with an initial capacitance of 248 pF at 0.1 Hz while measuring variations in capacitance. The test initiated with an applied constant displacement over a duration of 2 seconds to pre-stretch the specimen, followed by a harmonic displacement of 0.25 mm amplitude.

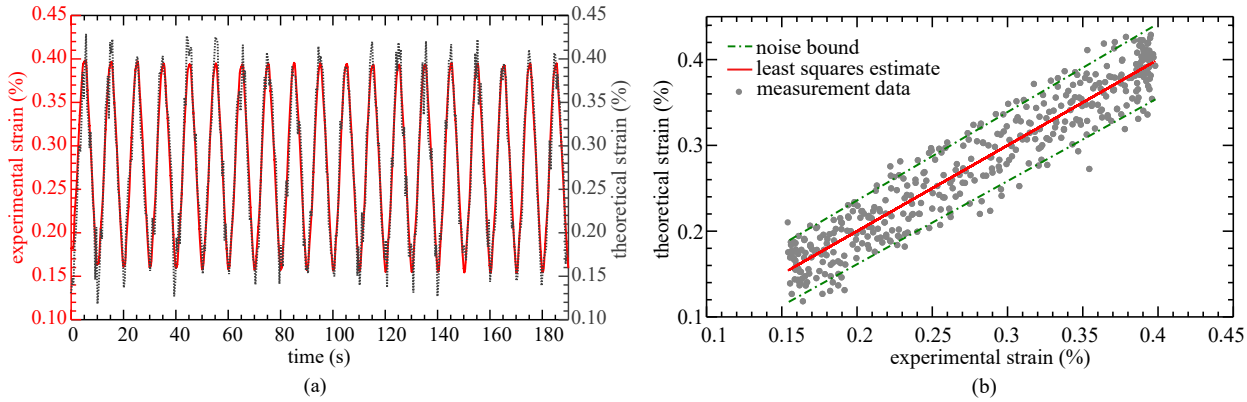

Figure 7: (a) Strain time histories at 0.1 Hz; and (b) theoretical versus experimental strains.

Figures 7(a) plots the theoretical strain computed from Equation (5) using an experimentally obtained gauge factor of $\lambda = 0.62$, and through a fit of the signal time histories using a least squares estimator. The gauge factor is lower than the values listed in Table 3, consistent with a prior study that demonstrated a loss in the gauge factor in dynamic modes that can be attributed to the frequency-dependence of the dielectric [38]. Figure 7(b) is a plot of the theoretical strain versus the experimental strain applied to the specimen, demonstrating the linearity of the sensor. The measurement noise bound is also shown (green dot-dashed lines), quantified as $\pm 65\mu\varepsilon$, giving a signal to noise ratio of 4.53.

After the study of the sensor's dynamic behavior under 0.1 Hz, the same sample was further subjected to a continuous 0.25 mm harmonic load with varying frequencies, starting at 0.25 Hz, followed by 0.5 and 1 Hz for 10 cycles each, where 1 Hz corresponded to the limit governed by the capacitance DAQ sampling rate (2.5 Hz). Figures 8(a) plots the time histories of the experimental and theoretical strain levels, where the gauge factor was computed under each harmonic inputs using a least squares estimator. Each individual gauge factors (λ =0.53, 0.44 and 0.43 at 0.25, 0.5, and 1 Hz, respectively) are indicated in the figure. Figure 8(b) reports each computed gauge factors, including the average from the quasi-static tests. Results show that the gauge factor decreases with increasing frequency and stabilizes, also consistent with previous work [38]. It follows that a field deployment of the CFRP capacitor will require calibration, increased precision, and an increased sampling rate of the capacitance to digital converter.

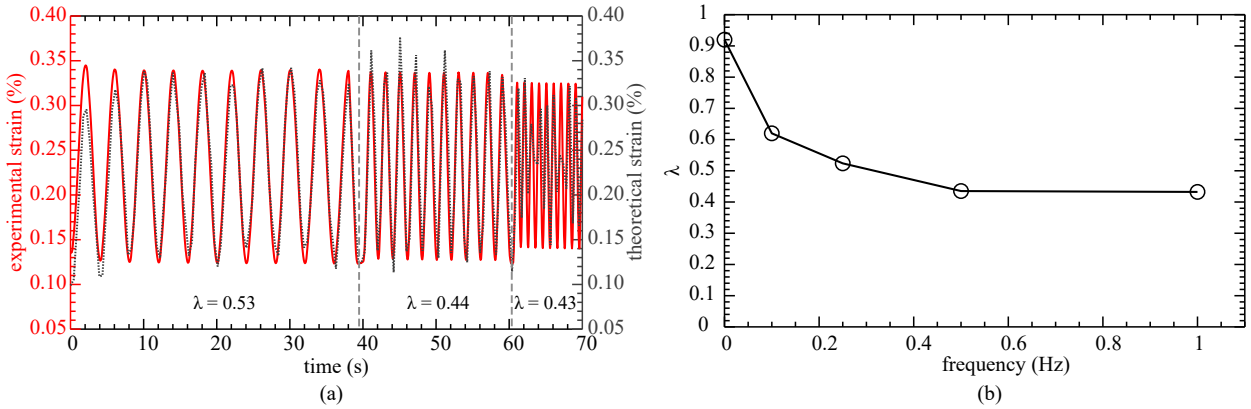

Figure 8: (a) Strain time histories at 0.25, 0.5, and 1 Hz; and (b) gauge factors versus frequency.

4. Conclusion

In this paper, a novel self-sensing CFRP was proposed. The multifunctional material is a capacitor, fabricated leveraging the CFRP for creating the parallel conductive plates and the epoxy filled with titania for creating the dielectric. Its sensing principle is based on a measurable change in capacitance provoked by strain. The background on the CFRP capacitor was presented, including a description of the materials used in its fabrication and a derivation of its sensing principle leading to the electromechanical model. After, the experimental methodology for characterizing the self-sensing CFRP was introduced, and the experimental results presented and discussed. The following conclusions can be drawn from this study:

1. The experiments initiated with the comparison of sensing properties between CFRP capacitor specimens with pristine and titania-filled epoxy. Enhanced CFRP capacitor performance that improves relative permittivity, electromagnetic noise rejection capabilities and long-term stability were achieved by doping the titania filler within the epoxy matrix.
2. The mechanical properties were obtained through the tensile tests under quasi-static loading. All five tested specimens demonstrated linear behavior until failure. The tensile modulus and strength depended on the amount of dielectric layer introduced into the CFRP capacitor. The results showed that the strength of CFRP capacitors calculated based on the thickness of the cured laminate is lower than that of the pristine CFRP laminate. Therefore, the strength and reinforcing effect of CFRP capacitors are affected by the amount of the dielectric layer.
3. The evaluation of the linearity of the sensor along with its gauge factor was conducted. Experimental results corroborated such linearity. An average gauge factor of 0.92 was obtained over the five specimens in free-standing modes.

4. Dynamic tests were conducted on a single specimen, and results showed that the sensor was able to measure strain up to 1 Hz, where the gauge factor decreased with the increasing frequency. It was also shown that the sensor, with its current fabrication process and associated data acquisition electronics, can measure strain within an error bound of $\pm 65\mu\varepsilon$ for a 0.1 Hz harmonic excitation.

Overall, the results presented in this paper demonstrate the promise of the CFRP capacitor at transforming the reinforcing material into a true multifunctional system capable of both strengthening and self-sensing. The self-sensing component could be useful, for example, at quickly evaluating the condition of a structure post-event, therefore enabling condition-based maintenance. The technology can also be used for SHM over a large area to provide discrete data over a continuous area. This can be done, for example, by deploying CFRP sensing strips strategically onto the monitored surface or producing an array of sensors by separating conductive CFRP plates with a nonconductive material without interrupting the dielectric.

Acknowledgments

The authors would like to acknowledge the financial support of the Midwest Transportation Center and National Science Foundation Grant No. 1069283 through the Integrative Graduate Education and Research Traineeship (IGERT) in Wind Energy Science, Engineering and Policy (WESEP) at Iowa State University. Also, the authors would like to thank BASF for donating CFRP materials; Douglas Wood and Owen Steffens from the Department of Civil, Construction, and Environmental Engineering and Dr. Joseph A. Schaefer from the Department of Aerospace Engineering at Iowa State University for their assistance with the experiments; Dr. Hantang Qin from Department of Industrial & Manufacturing Systems Engineering at Iowa State University for providing SEM images, and Yanhua Huang from the Department of Material Science Engineering for assisting in the fabrication of specimens.

References

References

[1] D. Agdas, J. A. Rice, J. R. Martinez, I. R. Lasa, Comparison of visual inspection and structural-health monitoring as bridge condition assessment methods, Journal of Performance of Constructed Facilities 30 (3) (2016) 04015049. doi:10.1061/(asce)cf.1943-5509.0000802.

[2] B. Culshaw, Health monitoring of aerospace structures: Smart sensor technologies and signal processing edited by w. staszewskiet al. john wiley and sons, the atrium, southern gate, chichester, west sussex, PO19 8sq, UK, 2004. 266pp. illustrated. $60. ISBN 0-470-84340-3., The Aeronautical Journal 111 (1125) (2007) 750. doi:10.1017/s0001924000087054.

[3] A. B. Noel, A. Abdaoui, T. Elfouly, M. H. Ahmed, A. Badawy, M. S. Shehata, Structural health monitoring using wireless sensor networks: A comprehensive survey, IEEE Communications Surveys & Tutorials 19 (3) (2017) 1403–1423. doi:10.1109/comst.2017.2691551.

[4] B. F. Spencer, H. Jo, K. A. Mechitov, J. Li, S.-H. Sim, R. E. Kim, S. Cho, L. E. Linderman, P. Moinzadeh, R. K. Giles, G. Agha, Recent advances in wireless smart sensors for multi-scale monitoring and control of civil infrastructure, Journal of Civil Structural Health Monitoring 6 (1) (2015) 17–41. doi:10.1007/s13349-015-0111-1.

[5] B. Glisic, D. Inaudi, Development of method for in-service crack detection based on distributed fiber optic sensors, Structural Health Monitoring: An International Journal 11 (2) (2011) 161–171. doi:10.1177/1475921711414233.

[6] A. Downey, S. Laflamme, F. Ubertini, Experimental wind tunnel study of a smart sensing skin for condition evaluation of a wind turbine blade, Smart Materials and Structures 26 (12) (2017) 125005. doi:10.1088/1361-665x/aa9349.

[7] A. D. B. Ferreira, P. R. Nóvoa, A. T. Marques, Multifunctional material systems: A state-of-the-art review, Composite Structures 151 (2016) 3–35. doi:10.1016/j.compstruct.2016.01.028.

[8] H. Abdel-Jaber, B. Glisic, Monitoring of long-term prestress losses in prestressed concrete structures using fiber optic sensors, Structural Health Monitoring: An International Journal (2018) 147592171775187doi:10.1177/1475921717751870.

[9] H. P. Konka, M. A. Wahab, K. Lian, On mechanical properties of composite sandwich structures with embedded piezoelectric fiber composite sensors, Journal of Engineering Materials and Technology 134 (1) (2012) 011010. doi:10.1115/1.4005349.

[10] Y. Goldfeld, O. Rabinovitch, B. Fishbain, T. Quadflieg, T. Gries, Sensory carbon fiber based textile-reinforced concrete for smart structures, Journal of Intelligent Material Systems and Structures 27 (4) (2015) 469–489. doi:10.1177/1045389x15571385.

[11] D. Bekas, Z. Sharif-Khodaei, M. Aliabadi, An innovative diagnostic film for structural health monitoring of metallic and composite structures, Sensors 18 (7) (2018) 2084. doi:10.3390/s18072084.

[12] B. Han, Y. Wang, S. Dong, L. Zhang, S. Ding, X. Yu, J. Ou, Smart concretes and structures: A review, Journal of Intelligent Material Systems and Structures 26 (11) (2015) 1303–1345. doi:10.1177/1045389x15586452.

[13] A. Meoni, A. D'Alessandro, A. Downey, E. García-Macías, M. Rallini, A. Materazzi, L. Torre, S. Laflamme, R. Castro-Triguero, F. Ubertini, An experimental study on static and dynamic strain sensitivity of embeddable smart concrete sensors doped with carbon nanotubes for SHM of large structures, Sensors 18 (3) (2018) 831. doi:10.3390/s18030831.

[14] F. Ubertini, A. D'Alessandro, A. L. Materazzi, S. Laflamme, A. Downey, Novel nanocomposite clay brick for strain sensing in structural masonry, in: 2017 IEEE International Conference on Environment and Electrical Engineering and 2017 IEEE Industrial and Commercial Power Systems Europe (EEEIC / I&CPS Europe), IEEE, 2017. doi:10.1109/eeeic.2017.7977598.

[15] A. Downey, A. D'Alessandro, S. Laflamme, F. Ubertini, Smart bricks for strain sensing and crack detection in masonry structures, Smart Materials and Structures 27 (1) (2017) 015009. doi:10.1088/1361-665x/aa98c2.

[16] I. Ray, G. C. Parish, J. F. Davalos, A. Chen, Effect of concrete substrate repair methods for beams aged by accelerated corrosion and strengthened with CFRP, Journal of Aerospace Engineering 24 (2) (2011) 227–239. doi:10.1061/(asce)as.1943-5525.0000030.

[17] A. M. Mahmoud, H. H. Ammar, O. M. Mukdadi, I. Ray, F. S. Imani, A. Chen, J. F. Davalos, Non-destructive ultrasonic evaluation of CFRP–concrete specimens subjected to accelerated aging conditions, NDT & E International 43 (7) (2010) 635–641. doi:10.1016/j.ndteint.2010.06.008.

[18] J. Abry, In situ detection of damage in CFRP laminates by electrical resistance measurements, Composites Science and Technology 59 (6) (1999) 925–935. doi:10.1016/s0266-3538(98)00132-8.

[19] A. Todoroki, J. Yoshida, Electrical resistance change of unidirectional CFRP due to applied load, JSME International Journal Series A 47 (3) (2004) 357–364. doi:10.1299/jsmea.47.357.

[20] I. Nam, S. Park, H. Lee, L. Zheng, Mechanical properties and piezoresistive sensing capabilities of frp composites incorporating cnt fibers, Composite Structures 178 (2017) 1–8. doi:10.1016/j.compstruct.2017.07.008.

[21] S. Blazewicz, B. Patalita, P. Touzain, Study of piezoresistance effect in carbon fibers, Carbon 35 (10-11) (1997) 1613–1618. doi:10.1016/s0008-6223(97)00120-6.

[22] S.-J. Joo, M.-H. Yu, E.-B. Jeon, H.-S. Kim, In situ fabrication of copper electrodes on carbon-fiber-reinforced polymer (CFRP) for damage monitoring by printing and flash light sintering, Composites Science and Technology 142 (2017) 189–197. doi:10.1016/j.compscitech.2017.02.011.

[23] M. Kupke, K. Schulte, R. Schüler, Non-destructive testing of FRP by d.c. and a.c. electrical methods, Composites Science and Technology 61 (6) (2001) 837–847. doi:10.1016/s0266-3538(00)00180-9.

[24] D. D. L. Chung, S. Wang, Carbon fiber polymer-matrix structural composite as a semiconductor and concept of optoelectronic and electronic devices made from it, Smart Materials and Structures 8 (1) (1999) 161–166. doi:10.1088/0964-1726/8/1/018.

[25] X. Luo, D. Chung, Carbon-fiber/polymer-matrix composites as capacitors, Composites Science and Technology 61 (6) (2001) 885–888. doi:10.1016/s0266-3538(00)00166-4.

[26] D. J. O'Brien, D. M. Baechle, E. D. Wetzel, Design and performance of multifunctional structural composite capacitors, Journal of Composite Materials 45 (26) (2011) 2797–2809. doi:10.1177/0021998311412207.

[27] H. Qian, A. R. Kucernak, E. S. Greenhalgh, A. Bismarck, M. S. P. Shaffer, Multifunctional structural supercapacitor composites based on carbon aerogel modified high performance carbon fiber fabric, ACS Applied Materials & Interfaces 5 (13) (2013) 6113–6122. doi:10.1021/am400947j.

[28] T. Carlson, L. ASP, An experimental study into the effect of damage on the capacitance of structural composite capacitors, Journal of Multifunctional Composites 2 (2) (2015) 71–77. doi:10.12783/issn.2168-4286/2.2/carlson.

[29] Z. Shen, H. Zhou, Mechanical and electrical behavior of carbon fiber structural capacitors: Effects of delamination and interlaminar damage, Composite Structures 166 (2017) 38–48. doi:10.1016/j.compstruct.2016.12.062.

[30] M. Amjadi, K.-U. Kyung, I. Park, M. Sitti, Stretchable, skin-mountable, and wearable strain sensors and their potential applications: A review, Advanced Functional Materials 26 (11) (2016) 1678–1698. doi:10.1002/adfm.201504755.

[31] X. Kong, J. Li, W. Collins, C. Bennett, S. Laflamme, H. Jo, A large-area strain sensing technology for monitoring fatigue cracks in steel bridges, Smart Materials and Structures 26 (8) (2017) 085024.

[32] A. A. Eddib, D. Chung, First report of capacitance-based self-sensing and in-plane electric permittivity of carbon fiber polymer-matrix composite, Carbon 140 (2018) 413–427. doi:10.1016/j.carbon.2018.08.070.

[33] W. Sun, X. Tan, M. R. Kessler, N. Bowler, Silicon/epoxy nanocomposites for capacitors as the energy storage element, in: 2013 Annual Report Conference on Electrical Insulation and Dielectric Phenomena, IEEE, 2013. doi:10.1109/ceidp.2013.6747423.

[34] X. Zhao, W. Hong, Z. Suo, Electromechanical hysteresis and coexistent states in dielectric elastomers, Physical Review B 76 (13). doi:10.1103/physrevb.76.134113.

[35] V. Tsouti, V. Mitrakos, P. Broutas, S. Chatzandroulis, Modeling and development of a flexible carbon black-based capacitive strain sensor, IEEE Sensors Journal 16 (9) (2016) 3059–3067. doi:10.1109/jsen.2016.2524508.

[36] A. Chen, Strength evaluation of honeycomb frp sandwich panels with sinusoidal core geometry, Ph.D. thesis, West Virginia University Libraries (2004).

[37] A. Chen, J. F. Davalos, Strength evaluations of sinusoidal core for FRP sandwich bridge deck panels, Composite Structures 92 (7) (2010) 1561–1573. doi:10.1016/j.compstruct.2009.10.039.

[38] H. Saleem, A. Downey, S. Laflamme, M. Kollosche, F. Ubertini, Investigation of dynamic properties of a novel capacitive-based sensing skin for nondestructive testing, Materials Evaluation 73 (10) (2015) 1384–1391.